Organic Electronics 13 (2012) 1765–1773

Contents lists available at SciVerse ScienceDirect

Organic Electronics

journal homepage: www.elsevier.com/locate/orgel

UV light-emitting electrochemical cells based on an ionic 2,2′-bifluorene derivative

Hsiao-Fan Chen [a], Chih-Teng Liao [b], Ming-Cheng Kuo [a], Yun-Shiuan Yeh [a], Hai-Ching Su [b,*], Ken-Tsung Wong [a,*]

[a] Department of Chemistry, National Taiwan University, Taipei 10617, Taiwan
[b] Institute of Lighting and Energy Photonics, National Chiao Tung University, Tainan 71150, Taiwan

ARTICLE INFO

Article history:
Received 22 March 2012
Received in revised form 11 May 2012
Accepted 21 May 2012
Available online 20 June 2012

Keywords:
Light-emitting electrochemical cells
Ultraviolet
Fluorene

ABSTRACT

UV light-emitting electrochemical cells (LECs) were, for the first time, achieved by the ionic 2,2′-bifluorene derivative, **1**, which was synthesized through covalent tethering of methylimidazolium moieties as pendent groups. LEC devices incorporating ionic bifluorene **1** without (Device **I**) and with (Device **III**) the presence of poly(methyl methacrylate) (PMMA) exhibited UV EL emissions centered at 388 and 386 nm with maximum external quantum efficiencies and power efficiencies of 1.06% and 7.44 mW W^{-1} for Device **III** and 0.15% and 1.06 mW W^{-1} for Device **I**, respectively. Transmission electron microscopy (TEM) images showed that **1** tends to form nanospheres due to amphiphilic nature. The presence of PMMA unified the size of nanospheres which greatly reduced the void area in films, suppressing the current leakage and enhancing the device efficiency. Furthermore, thicker thickness of the emissive layer of LECs increases the distance between carrier recombination zone and electrodes to avoid exciton quenching. Thus, a sevenfold increase in device efficiency was obtained in thicker UV LECs containing PMMA (Device **III**) as compared to thinner UV LECs based on neat films of **1** (Device **I**). The EL emissions in the UV region are successfully achieved by LECs based on **1**, which are so far the shortest emission wavelength achieved in LECs.

1. Introduction

Solid state light-emitting electrochemical cells (LECs) possess solution-processable simple device architecture and high compatibility with air-stable electrodes such as gold, silver, and aluminum [1]. In LEC devices, electrochemically doped regions induced by spatially separated ions under an applied voltage generate ohmic contacts with electrodes, resulting in balanced carrier injection and low operating voltages and, consequently, high power efficiencies. These promising advantages render this type of electroluminescent device competitive with conventional organic light-emitting diodes (OLEDs) as a cost-effective alternative for display and lighting [2].

Among the reported literatures of small-molecule LECs, most of them are based on cationic transition metal complexes (CTMCs). LECs based on CTMCs have shown several advantages including (i) high compatibility with ionic electrolytes imparted by intrinsic ionicity of CTMCs, (ii) high electroluminescent (EL) efficiencies due to phosphorescent nature, and (iii) tunable emission colors [3]. Particularly, the most widely used CTMCs for single-component LEC devices are based on cationic iridium(III) complexes owing to their facile synthetic pathways and a full coverage of emission wavelength in the visible region by tailoring the structures of their chelating ligands [4]. However, intrinsic narrow energy gaps and accessible non-radiative ligand

* Corresponding authors. Tel.: +886 6 3032121x57792; fax: +886 6 3032535 (H.C. Su), tel.: +886 2 33661665; fax: +886 2 33661667 (K.-T. Wong).
E-mail addresses: haichingsu@mail.nctu.edu.tw (H.-C. Su), kenwong@ntu.edu.tw (K.-T. Wong).

1566-1199/$ - see front matter © 2012 Elsevier B.V. All rights reserved.
http://dx.doi.org/10.1016/j.orgel.2012.05.050

field states of cationic iridium complexes substantially restrict their practical use for achieving blue-emitting LEC devices [5]. To achieve saturated blue-emitting LEC devices, we have successfully demonstrated so far the bluest electroluminescence from the LEC based on ionic terfluorene derivative [6]. The ionic fluorescent emitter was achieved by covalent tethering of 1-methylimidazolium moieties as pendant groups, rendering a hydrophobic terfluorene core bearing movable anions to form homogeneous films through spin-coating. The efficient and successful strategy for accomplishing blue-emitting LEC propelled us to further explore the molecules with larger energy gaps, potentially realizing UV excitation light source for light-emitting devices.

The development of wide-gap materials is rather limited to a few functionalized structural features such as materials containing carbazoles [7] and silane [8] moieties in order to obtain a confined conjugation length. The emissions of these wide-gap materials are generally above 400 nm, i.e., violet-blue emission. However, limited π-conjugation considerably complicates the molecular design since it also constraints the molecular size and coplanarity which are related to the molecular morphological stability and luminescent properties. It is rather difficult to construct a molecule which meets most general requirements for optoelectronic materials such as high thermal stability, good carrier mobility, and ionic (for LEC application) in a limited conjugation and dimension. As a result, with meticulous selection on the wide-gap chromophores, we have demonstrated several UV OLEDs based on 2,2′-bifluorene derivatives with remarkable short emission wavelength centered at 370 nm and external quantum efficiency up to 3.6% [9]. Distinguish and efficient UV emission below 400 nm is rarely reported for organic materials and has never been done for LEC application. Herein, we present the first UV LEC achieved by 2,2′-bifluorene derivative with ionic pendant 1-methylimidazolium moieties, achieving the EL as short as 386 nm. The successful demonstration of UV LEC once again proved that our judicious molecular design strategy for ionic emitters is much suitable for LEC application.

2. Results and discussion

2.1. Synthesis

Scheme 1 outlines the synthetic routes of the ionic bifluorene (**1**). We obtained the bromo-substituted 2,2′-bifluorene **1-Br** after homo-coupling *via* modified one-pot Suzuki coupling [10] of 2-bromo-9,9-bis(6-bromohexyl)fluorene (**2**) [11] in 46% yield. After treating **1-Br** with excess amount of 1-methylimidazole followed by ion-exchange with potassium hexafluorophosphate, we isolated compounds **1** in 81% yield.

2.2. Photophysical properties

Fig. 1 depicts the UV–Vis absorption and PL spectra of **1** in solution (acetonitrile, 10^{-5} M) and in the form of neat films. The excitation wavelength is 280 nm. Table 1 summarizes the photophysical data. To increase the film quality, we also dispersed compound **1** into inert poly(methyl methacrylate) (PMMA) which can efficiently fill out the defect sites of the film to diminish the current leakage of the device [12]. Thus, the emission properties of compound **1** dispersed in PMMA (10 wt%) is also examined. In solution, **1** exhibits an absorption signal centered at 328 nm, which we assign to the lowest π–π* transition of the bifluorene backbone. In its PL spectrum, **1** reveals intense fluores-

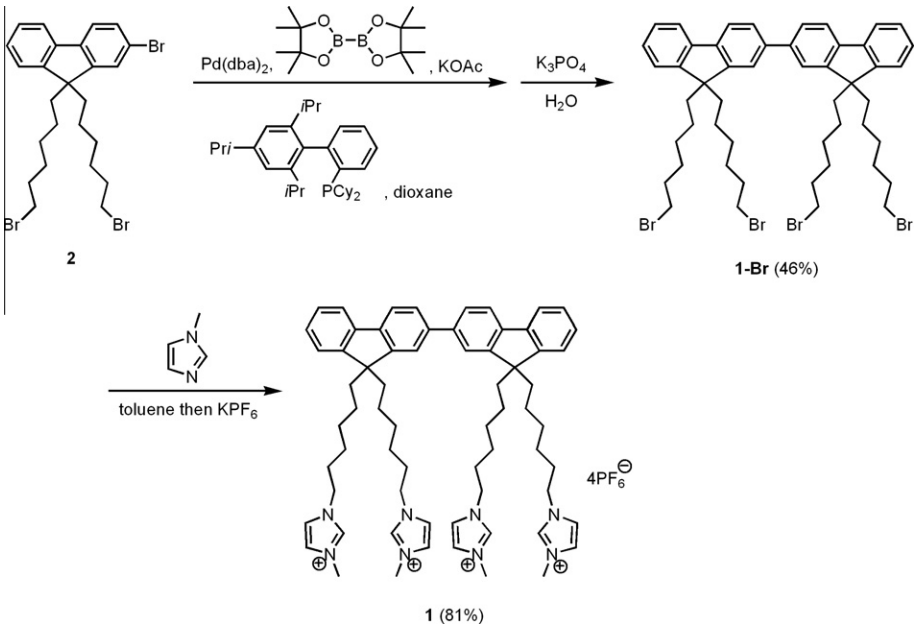

Scheme 1. Synthesis of **1**.

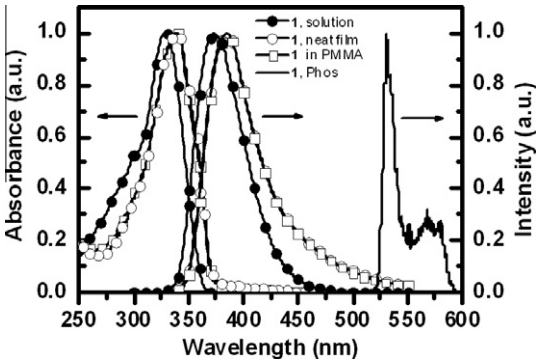

Fig. 1. Absorption (left-hand axis) and PL (right-hand axis) spectra of **1** in MeCN solution (10^{-5} M) and in neat film or dispersed in PMMA film (10 wt%) and the phosphorescence (Phos, right-hand axis) spectrum of **1** in EtOH solutions at 77 K. The excitation wavelength is 280 nm.

cence with an emission maximum centered at 373 nm and an excellent quantum yield of 100%. These values correspond with the published results of bifluorene derivatives [9]. Both absorption and PL spectra of **1** in neat films are red-shifted by *ca.* 10 nm as compared with those in solutions due to enhanced molecular polarization effect in the solid state [13]. Interestingly, by adding 10 wt% PMMA in the films of **1**, no significant change is observed for the absorption and PL spectra as compared to that without PMMA, indicating that **1** is still in the form of small aggregates instead of completely dispersion in PMMA. The amphiphilic property of **1**, imparted by solvophilic imidazolium and solvophobic bifluorene backbone, renders a substantial hydrophobic effect to potentially organize nano-scale architectures by non-covalent interactions [14]. The addition of PMMA is speculated to give certain extent of separation to these small aggregates, evidenced by the identical absorption and PL spectra for **1** with and without the presence of PMMA, respectively. The triplet energy of **1** (2.33 eV) was determined from the highest energy vibronic sub-band of the phosphorescence spectra recorded in EtOH at 77 K. Similar triplet energies can be also obtained in MeCN (2.32 eV) and acetone (2.33 eV) at 77 K due to retarded solvent relaxation process in the triplet excited state. The low E_T value indicates a significant exchange of stabilization energy of the bifluorene chromophore.

2.3. Cyclic voltammetry

Fig. 2 displays the electrochemical characteristics of **1**, as probed by cyclic voltammetry. A quasi-reversible oxidation potential [at +1.04 V (vs. Fc/Fc^+)] in acetonitrile (0.1 M nBu$_4$NPF$_6$ as supporting electrolyte) and a quasi-reversible reduction potential [at −2.66 V (vs. Fc/Fc^+)] in acetonitrile (0.1 M nBu$_4$NClO$_4$ as supporting electrolyte) were distinctly observed for **1**. The corresponding highest occupied molecular orbital (HOMO) and lowest unoccupied molecular orbital (LUMO) levels are −5.84 and −2.14 eV, respectively. We unambiguously assign both the oxidation and reduction peaks to electron transfer processes that occurred on the bifluorene backbone, consistent with the published bifluorene derivatives [9]. The reduction peak is less reversible in terms of a lower peak current in the reverse scan as compared with that of oxidation. It is presumably due to the pendent imidazolium units interacting with the reduced species and, consequently, retarding the diffusion toward the electrode [4g]. The multi-cathodic scans yielded identical reduction peaks in the reverse cathodic scan and no additional peaks were appeared in the 2nd and 3rd scans (Fig. 2, inset), indicating that the poor reversibility in the reduction peak does not involve a chemically irreversible step. Compound **1** possesses a more positive oxidation and a less negative reduction than those of neutral bifluorene derivatives (where the oxidation and reduction potentials are in a range of +0.89 to +0.99 V and −2.74 to −2.94 V, respectively, vs. Fc/Fc^+) [9a], suggesting a substantial inductive effect given by methylimidazolium units.

2.4. Electroluminescence

To examine the electroluminescence properties of **1**, LEC devices based on **1** were fabricated and the device characteristics are summarized in Table 2. The device structures are glass/indium tin oxide (ITO) (120 nm)/poly(3,4-ethylenedioxythiophene):poly(styrene sulfonate) (PEDOT:PSS) (30 nm)/emissive layer/Ag (100 nm) (where

Table 1
Physical properties of **1**.

	$\lambda_{max,PL}$ (nm)[b]		PLQY[c]		$E^{ox}_{1/2}$ (V)[d]	$E^{red}_{1/2}$ (V)[e]	$E_{1/2}$ (V)[f]	E_T (eV)
	Solution[a]	Film	Solution[a]	Film				
1	373	385	1.00	0.45	+1.04[g]	-2.66[h]	3.70	2.33
1 with 10 wt% PMMA	–	385	–	0.41	–	–		–

All potentials were recorded vs. Ag/AgCl (saturated) as a reference electrode. A glassy carbon electrode was used as the working electrode; scan rate 200 mV/s.

[a] Measured in MeCN (10^{-5} M) at room temperature.
[b] PL peak wavelength.
[c] Photoluminescence quantum yields.
[d] Oxidation potential vs. ferrocene/ferrocenium redox couple.
[e] Reduction potential vs. ferrocene/ferrocenium redox couple.
[f] The electrochemical gap $E_{1/2}$ is the difference between $E^{ox}_{1/2}$ (V) and $E^{red}_{1/2}$ (V).
[g] 0.1 M TBAPF6 in MeCN.
[h] 0.1 M TBAP in MeCN.

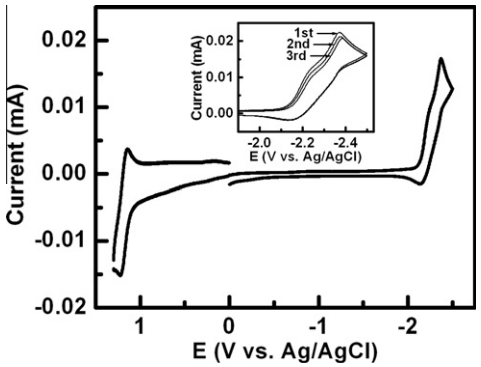

Fig. 2. Cyclic voltammogram of compound **1**. All potentials were recorded vs. Ag/AgCl (saturated) as a reference electrode. Repeated cyclic voltammograms (3 cycles) are shown in the inset. A glassy carbon electrode was used as the working electrode; scan rate 200 mV/s.

the emissive layer was a neat film of **1** (250 nm) for Device **I** and thin films of **1** containing 10 wt% poly(methyl methacrylate) (PMMA) with thicknesses of 250, 350 and 500 nm for Devices **II**–**IV**, respectively). In Devices **II–IV**, PMMA was added to improve film quality and thus to decrease the leakage current during device operation, enhancing device efficiency [15]. The polymer PMMA was chosen due to its inert electrical properties, high transparency at the emission spectrum of **1** and moderate miscibility with ionic materials. Measurements of all device properties were performed under constant bias voltages (4.2 and 4.6 V). Ten different devices of each type (**I–IV**) were measured and the typical device-to-device variation in electrical properties is within *ca.* ±5%. Fig. 3 compares the EL spectra of the LEC devices under 4.2 V and the PL spectra of their emissive layers. The similarity of the EL spectra of all devices indicates that the addition of PMMA did not significantly alter the EL of **1**. Slight discrepancies in intensities of EL vibronic peaks between LEC devices based on films of **1** without and with PMMA may be attributed to altered molecular potential energy surfaces of **1** in media with different polarities [16] under applied electric fields. Notably, the signals in the EL spectra are slightly broadened at 420–500 nm relative to those in the PL spectra. It is primarily related to thermal rearrangement of the molecules and, consequently, the enhanced formation of intermolecular excimer species [17]. Since such effect is not significant in LEC devices based on **1**, LEC devices exhibited EL emissions centered at UV region (λ_{max} = 386 and 388 nm for LEC devices based on films of **1** without and with PMMA, respectively), which are the bluest EL emissions ever reported for LECs. The Commission Internationale de l'Eclairage (CIE) coordinates for the EL spectra of UV LECs without and with PMMA are (0.162, 0.104) and (0.164, 0.103), respectively. Similar CIE coordinates of EL spectra for UV LECs and previously reported deep-blue LECs based on an ionic terfluorene derivative [6] result from that human eyes have little response to UV light at wavelength <400 nm and only visible part of EL emission is responsible for calculation of CIE coordinates, which are not suitable for use in evaluating the quality of UV light sources. For instance, compared with the EL spectra of deep-blue LECs (λ_{max} = 424 nm, full width at half maximum (FWHM) = 95 nm) [6], the EL spectra of UV LECs based on **1** exhibit a 40 nm blue-shifted peak wavelength and a narrower FWHM of *ca.* 70 nm. Thus, the percentage of UV EL emission (<400 nm) of total EL spectra of UV LECs is up to *ca.* 37% while UV emission in EL spectra of deep-blue LECs is only 3.5%. In view of these results, UV LECs based on **1** show significantly more proportion of UV EL emission in comparison with the bluest LECs ever reported [6] and consequently confirm that compound **1** is a promising candidate for use as a UV-emitting material in LECs.

Fig. 4(a)–(d) present the time-dependent light output and current densities when operated under 4.2 and 4.6 V for Devices **I**–**IV**, respectively. The driving voltages are chosen to be close to the energy gap of **1** (3.7 eV in solutions,

Table 2
LEC device characteristics.

Device[a]	Bias voltage (V)	$\lambda_{max,EL}$ (nm)[b]	CIE (x, y)[c]	t_{max} (min)[d]	J_{max} (mA cm^{-2})[e]	L_{max} (μW cm^{-2})[f]	B_{max} (cd m^{-2})[g]	$\eta_{ext,max}$ (%)[h]	$\eta_{p,max}$ (mW W^{-1})[i]	Lifetime (min)[j]
I	4.2	386	(0.162, 0.104)	5.0	2.27	1.87	0.34	0.15	1.06	5.8
	4.6			4.0	4.30	3.31	0.54	0.14	0.90	3.3
II	4.2	388	(0.164, 0.103)	4.8	1.51	4.15	0.66	0.66	4.66	4.9
	4.6			3.2	3.78	6.96	1.08	0.64	4.03	3.0
III	4.2	388	(0.164, 0.103)	6.7	1.06	5.01	0.80	1.06	7.44	9.7
	4.6			6.3	2.76	10.23	1.59	0.79	4.98	6.2
IV	4.2	388	(0.164, 0.103)	12.8	0.48	1.12	0.18	0.69	4.86	13.2
	4.6			10.0	0.98	1.58	0.25	0.63	4.03	10.3

[a] Device structures: Glass/ITO (120 nm)/PEDOT:PSS (30 nm)/emissive layer [Device **I**: 100 wt% **1** (250 nm), Device **II**: 90 wt% **1** + 10 wt% PMMA (250 nm), Device **III**: 90 wt% **1** + 10 wt% PMMA (350 nm) and Device **IV**: 90 wt% **1** + 10 wt% PMMA (500 nm)/Ag (100 nm)].
[b] EL peak wavelength.
[c] CIE coordinates of EL spectra.
[d] Time required to reach the maximal light output.
[e] Maximal device current density achieved at a constant bias voltage.
[f] Maximal light output achieved at a constant bias voltage.
[g] Maximal brightness achieved at a constant bias voltage.
[h] Maximal external quantum efficiency achieved at a constant bias voltage.
[i] Maximal power efficiency achieved at a constant bias voltage.
[j] The time for the light output of the device to decay from the maximum to half of the maximum under a constant bias voltage.

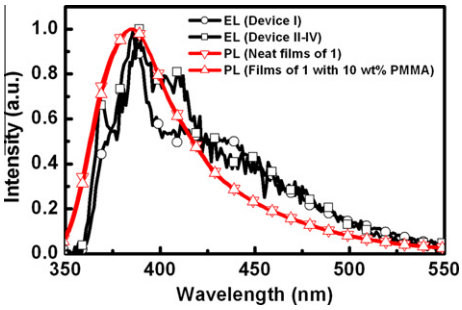

Fig. 3. EL spectra of UV LECs at 4.2 V. PL spectra of the emissive layers are presented for comparison.

Table 1) to improve the device stability [4h]. Since all LECs exhibit significant UV EL emissions, brightness, which is calculated from the visible part of EL spectra, would not be suitable for use in evaluating the light output of UV LECs and optical power was measured instead. All LEC devices exhibited similar electrical characteristics. The light output and device current first increased with time after the bias was applied, reaching maximum values before undergoing gradual decreases over time. The time required for the light output to reach its maximum value decreased as the bias voltage increased (Table 2), presumably because a higher accumulation rate of mobile ions facilitated the formation of electrochemically doped regions under a higher electric field. Devices **I** and **II** showed similar time required to reach the maximum light output under the same bias voltage (e.g., 5.0 and 4.8 min for Devices **I** and **II**, respectively, at 4.2 V). This result indicates that addition of inert PMMA could not significantly alter the ionic mobility of the emissive layer possibly due to a high density of mobile ions in the films of **1** ($4PF_6^-$ anions per molecule). However, Device **II** exhibited a lower maximum device current density under the same bias voltage as compared to Device **I** (e.g., 2.27 and 1.51 mA cm^{-2} for Devices **I** and **II**, respectively, at 4.2 V). Since the emissive layers of both devices have similar thicknesses (250 nm), lowered device current density of Device **II** may be attributed to impeded charge hopping between dispersed **1** in PMMA matrix. Furthermore, improved film quality by adding PMMA may also reduce the leakage current of the emissive layer, rendering a lower device current. In spite of a lowered device current was obtained in Device **II**, it exhibited a much higher light output than Devices **I** under the same bias voltage (Fig. 4(a) and (b)). It reveals that a significant amount of leakage current, which can not contribute to device light output, would be reduced due to improved film quality induced by addition of PMMA and thus significantly improved device efficiency resulted in a higher light output even under a lower device current. Since Device **II** can generate more light output under a lower electrical power input (the same bias voltage but lower device current) as compared to Devices **I**, addition of PMMA in the emissive layer is confirmed to improve the device performance of UV LECs based on **1**. Further increase in the thickness of the emissive layer leads to even lower device current and slower device response (Devices **III** and **IV**, Table 2). Longer time is required for accumulation of enough mobile ions near electrodes to build up electrochemically doped layer due to a reduced electric field in a thicker emissive layer. In addition, a reduced electric field also results in lowered device current.

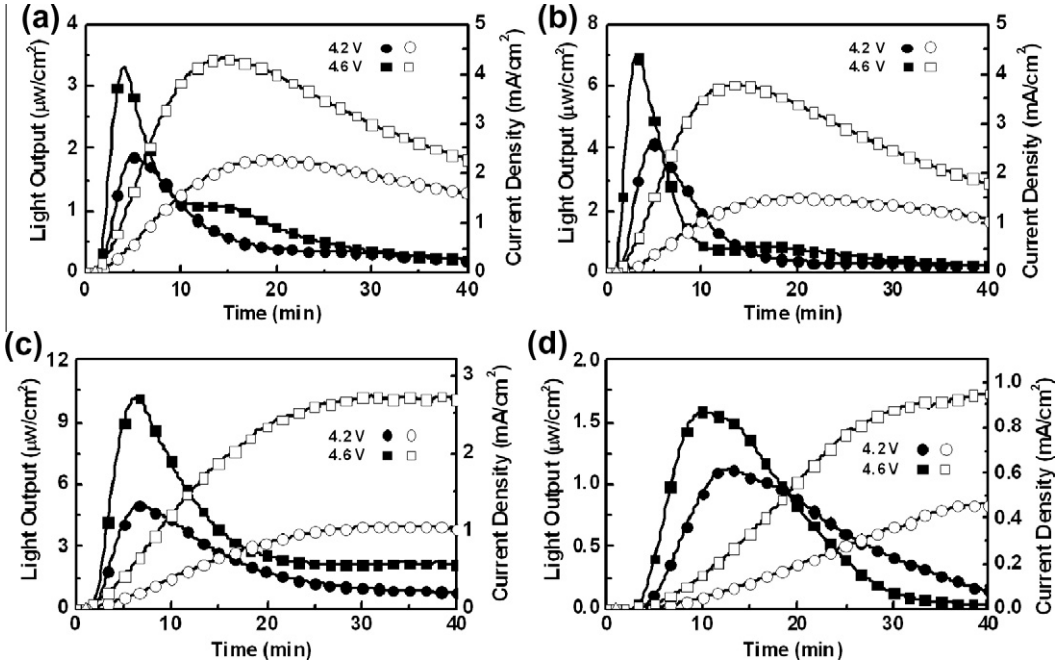

Fig. 4. Light output (solid symbols) and current density (open symbols) plotted with respect to time under a constant bias voltage of 4.2 and 4.6 V for (a) Device **I**, (b) Device **II**, (c) Device **III** and (d) Device **IV**.

The decreases in light output and current densities over time after reaching the maximum values are associated with degradation of the emissive material during LEC operation. The maximum light output and current density obtained in the first measurement were not fully recoverable in subsequent measurements, even under the same driving conditions. Under a constant bias, the lifetime of each device, defined as the time required for the light output of the device to decay from the maximum value to half of the maximum value, decreased upon increasing the bias voltage. For instance (Table 2), the lifetime of Device **I** (Device **II**) decreased from 5.8 to 3.3 min (4.9 to 3.0 min) upon increasing the bias voltage from 4.2 to 4.6 V. Several mechanisms have been reported to be responsible for device degradation of LECs. For LECs based on CTMCs, device degradation results from that higher current density induced by a higher bias voltage led to a higher rate of irreversible multiple oxidation and subsequent decomposition of the emissive material, thereby accelerating the degradation of the LEC devices [18a,b]. For polymer LECs, device degradation has been attributed to electrochemical overdoping and/or side reactions in the doped polymer near the electrodes [18c,d]. In addition, for LECs based on an ionic fluorene derivative, degradation due to keto defect [18e] would be another possible reason for their short device lifetimes. It is noted that the differences in the device lifetimes of Device **I** (without PMMA) and Device **II** (with 10 wt% PMMA) are not significant (*ca.* 10% and 15% at 4.6 and 4.2 V, respectively). Such differences are within the experimental errors due to thickness variation of spin-coated thin films. Hence, short device lifetimes mainly result from the intrinsic electrochemical characteristics of **1** and the PMMA may play a minor role in device degradation of UV LECs based on **1**. The lifetimes of UV LECs with thicker emissive layers (Devices **III** and **IV**, Table 2) are longer since reduced current densities mitigate degradation rates of the emissive material. Thus, increasing device thickness is beneficial in improving device stability of UV LECs.

Fig. 5(a)–(d) presents the time-dependent external quantum efficiencies (EQEs) and corresponding power efficiencies operated under 4.2 and 4.6 V for Devices **I**–**IV**, respectively. All devices exhibited similar time evolutions of their device efficiencies. Immediately after a forward bias was applied, the EQE was rather low because of unbalanced carrier injection. During the formation of the doped regions near the electrodes, the balance of the carrier injection was improved and, accordingly, the EQE of the device increased rapidly. The peak EQE and peak power efficiency were 0.15% and 1.06 mW W^{-1}, respectively, for Device **I** under 4.2 V and 0.66% and 4.66 mW W^{-1}, respectively, for Device **II** under 4.2 V. The device efficiency of Device **II** is much higher than that of Device **I** under the same bias voltage. Since the photoluminescence quantum yields (PLQYs) of **1** in the films with and without PMMA are similar (0.41 and 0.45, respectively, Table 1), enhanced device efficiency of LECs based on **1** containing 10 wt% PMMA cannot be attributed to reduced self-quenching of **1** dispersed in PMMA matrix. Possible reason for this phenomenon would come from reduced device current due to impeded charge hopping between dispersed molecules in PMMA matrix. Lower current density suppresses collision-induced exciton dissociation and consequently reduces efficiency roll-off. Thus, a higher device efficiency

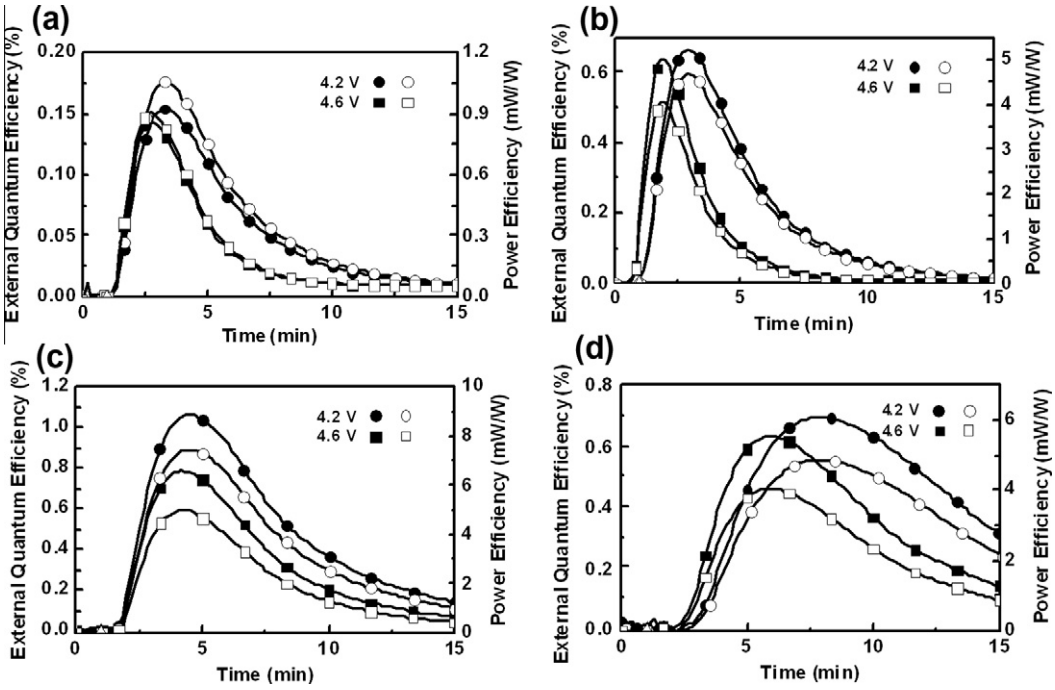

Fig. 5. EQE (solid symbols) and power efficiency (open symbols) plotted with respect to time under a constant bias voltage of 4.2 and 4.6 V for (a) Device **I**, (b) Device **II**, (c) Device **III** and (d) Device **IV**.

would be obtained at a lower device current density. In addition, reduced leakage current of the emissive layer due to improved film quality by adding PMMA may also enhance device efficiency. However, the maximum EQEs (0.66%) of Device **II** are much lower than the upper limit (~2%) that one would expect from the PLQYs of the films of **1** containing 10 wt% PMMA (0.41, Table 1), when considering fluorescent spin statistics (*ca.* 25%) and an optical out-coupling efficiency of *ca.* 20% from a typical layered light-emitting device structure. To further enhance device efficiency, the thicknesses of the emissive layer (**1** with 10 wt% PMMA) were enhanced to 350 and 500 nm for Device **III** and **IV**, respectively. The EQE and power efficiency of Device **III** under 4.2 V reached 1.06% and 7.44 mW W^{-1}, respectively, which represent a 1.6 times enhancement compared to those of Device **II** based on a thinner emissive layer (250 nm) with the same material components. Compared with UV LECs based on thinner neat films (250 nm) of **1** (Device **I**), sevenfold enhancement in device efficiency was obtained for Device **III**. When a constant bias is applied to LEC devices, the p- and n-type doped layers keep extending and the carrier injection efficiency is continuously enhanced. Therefore, the carrier recombination zone may keep moving closer to one electrode due to discrepancy in electron and hole mobilities, which would induce exciton quenching, deteriorating light output and device efficiency [4i]. A thicker emissive layer is beneficial in keeping the carrier recombination zone away from electrodes. Hence, exciton quenching near electrodes would be mitigated and device efficiencies would thus be enhanced. However, further increase in thickness of the emissive layer, e.g., 500 nm for Device **IV,** results in deteriorated device efficiencies as well (peak EQE = 0.69% under 4.2 V, Table 2). Even thicker emissive layer leads to significantly reduced electric field and consequently alters field-dependent carrier mobilities of the emissive material. Carrier balance may be affected due to altered carrier mobilities. Furthermore, a low electric field may not be capable of accumulating enough mobile ions near electrodes to properly build up electrochemically doped layers for efficient carrier injection, rendering deteriorated carrier balance as well. The best EQE obtained in UV LECs based on **1** (1.06%, Device **III**) reached *ca.* 50% of the upper limit (~2%) that one would expect from the PLQYs of the films of **1** containing 10 wt% PMMA (0.41, Table 1) when fluorescent spin statistics of *ca.* 25% and an optical out-coupling efficiency of *ca.* 20% are estimated. These results reveal that LEC devices based on **1** can exhibit UV EL emissions with moderate device efficiencies, making them potential candidates of UV emitting materials for use in LECs.

In addition to the intrinsic physical properties of **1** that mainly affect the device performance, the preferable self-assembled aggregation state of **1** induced by amphiphilic nature (consisted of hydrophobic bifluorene and hydrophilic methylimidazolium) may bring out another issue in solid-state device. We used transmission electron microscopy (TEM) to probe the self-assembled aggregation behavior of **1** developed from its acetonitrile solutions (0.1 mM) with and without 10 wt% PMMA (Fig. 6). TEM samples were prepared by evaporating the solution of molecules **1** (10 μL, 0.1 mM) onto a copper grid (200 mesh). The self-assembly of **1** from acetonitrile solution led to the formation of nanospheres with the diameters ranging from *ca.* 150 nm to 1.6 μm (Fig. 6, left). The self-assembled nanostructures of **1** were not altered in the presence of PMMA, suggesting a substantial aggregation tendency of amphiphilic **1** toward nanospheres. Notably, the nanospheres were dispersed into a layer of PMMA membrane with a significant narrow in their size distribution (*ca.* 200–400 μm, Fig. 6, right). The large porous structure in the background was attributed to water condensation during the solvent evaporation process [19]. The uniformity of nanospheres in the presence of PMMA may account for the superior device performance because it diminishes the empty regions in films which could abundantly exist when the film is consisted of nanospheres with large discrepancy in size. As a result, it is concluded that any organic material with ionic character would be potential to form nanoscale self-assembled aggregate due to amphiphilic property. It is known that an amorphous film is always required for light-emitting devices to avoid any preferable hole and/or electron channels. Materials which possess certain degree of aggregation tendency are not considered as good candidates. For example, ordered aggregation has been reported

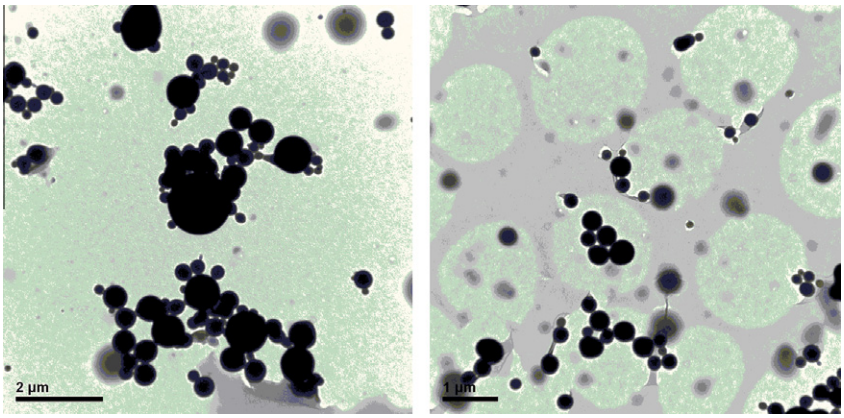

Fig. 6. TEM images of **1** (left) and with 10 wt% PMMA (right).

to result in significant anisotropic carrier mobility, which would affect carrier balance of devices [20]. Fortunately, spherical structure does not have any directional repetition and can still be seen as "amorphous" to a certain extent. In our cases, the size uniformity of the nanospheres is crucial for the device performance in terms of the extent of current leakage.

3. Conclusion

We have synthesized a UV-emitting ionic bifluorene derivative, **1**, that realized the unprecedented UV-emitting LECs. We achieved the essential ionic character required for LECs by chemically tethering methylimidazolium moieties as pendent groups to the bifluorene. Incorporating the inert PMMA in the emitting layer of Device **II** impeded charge hopping between dispersed molecules as well as improved the film quality, leading to a reduced current density and current leakage. Furthermore, the thickness of the emissive layer was increased to avoid exciton quenching near electrodes and thus to enhance device efficiency. The highest peak EQE was over seven times larger in the device based on thicker films with PMMA (350 nm, Device **III**) than that based on thinner films without PMMA (250 nm, Device **I**). The peak EQE and power efficiency of Device **III** were 1.06% and 7.44 mW W^{-1}, respectively, at 4.2 V. TEM images showed that **1** tends to form nanospheres due to amphiphilic nature. The presence of PMMA unified the size of nanospheres which greatly reduced the void area in films, suppressing the current leakage efficiently. All LEC devices based on **1** exhibited UV EL emissions at *ca.* 386 nm, which are the first example of UV LEC ever reported.

4. Experimental section

4.1. General experiments

^1H and ^{13}C NMR spectra of compounds were collected on a 400 MHz spectrometer at room temperature. Photophysical characteristics of complexes in solutions were collected at room temperature by using 10^{-5} M acetonitrile (MeCN) solutions of all compounds, which were carefully purged with nitrogen prior to measurements. The thickness of spin-coated films was measured by profilometry. UV–visible absorption spectra were recorded on a spectrophotometer (HITACHI U2800A). PL spectra were measured with a fluorescence spectrophotometer (HITACHI F9500). PLQYs for solution and thin-film samples were determined with a calibrated integrating sphere system (HAMAMATSU C9920). Oxidation and reduction potentials of all complexes were determined by cyclic voltammetry (CV) at a scan rate of 200 mV/s in MeCN solutions (1.0 mM). A glassy carbon electrode and a platinum wire were used as the working electrode and the counter electrode, respectively. All potentials were recorded versus the Ag/AgCl (sat'd) reference electrode and calibrated with the ferrocene/ferrocenium redox couple. Oxidation CV was performed using 0.1 M tetra-*n*-butylammonium hexafluorophosphate ($TBAPF_6$) in MeCN. For reduction CV, 0.1 M tetra-*n*-butylammonium perchlorate (TBAP) in MeCN was used as the supporting electrolyte. Samples for TEM were drop-casted onto a 200 mesh copper grid coated with formvar film stabilized with vacuum-evaporated carbon and dried under air. The samples were examined in electron microscopes operating at 75 kv (Hitachi H-7650).

4.2. Synthesis of 9,9,9′,9′-tetrakis(3-bromohexyl)-2,2′-bifluorene (**1-Br**)

A mixture of 2-bromo-9,9-dipropylfluorene (1.8 g, 3.15 mmol), bis(pinacolato)diborane (400 mg, 1.58 mmol), tris(dibenzylideneacetone)dipalladium(0) (15 mg, 0.02 mmol), 2-dicyclohexylphosphino-2′,4′,6′-triisopropylbiphenyl (30 mg, 0.06 mmol), potassium phosphate monohydrate (2.2 mg, 9.45 mmol), and dioxane (15 mL) was refluxed for 16 h. After dioxane was removed by rotary evaporation, the reaction mixture was extracted with CH_2Cl_2 and dried over $MgSO_4$. The crude product was purified by column chromatography on silica gel (CH_2Cl_2/hexane = 1/5) to afford pure **1-Br** (708 mg, 46%) as a white solid. ^1H NMR ($CDCl_3$, 400 MHz) δ7.78 (d, J = 7.6 Hz, 2H), 7.74 (d, J = 7.6 Hz, 2H), 7.65 (dd, J = 7.6, 1.6 Hz, 2H), 7.60 (s, 2H), 7.38–7.30 (m, 6H), 3.28 (t, J = 6.8 Hz, 8H), 2.08–2.03 (m, 8H), 1.65 (quin, J = 7.2 Hz, 8H), 1.23 (quin, J = 7.2 Hz, 8H), 1.11 (quin, J = 7.2 Hz, 8H), 1.74–0.69 (m, 8H); ^{13}C NMR ($CDCl_3$, 100 MHz) δ151.1, 150.6, 140.8, 140.4, 140.4, 127.1, 126.9, 126.2, 122.8, 121.2, 120.0, 119.8, 55.1, 40.2, 33.9, 32.6, 29.0, 27.7, 23.6; HRMS (m/z, FAB^+) Calcd for $C_{50}H_{62}{}^{79}Br_4$ 978.1585, found: 978.1586; Calcd for $C_{50}H_{62}{}^{79}Br^{81}Br_3$ 980.1565, found: 980.1561; Calcd for $C_{50}H_{62}{}^{79}Br_2{}^{81}Br_2$ 982.1544, found: 982.1525; Calcd for $C_{50}H_{62}{}^{79}Br_3{}^{81}Br$ 984.1524, found: 984.1541; Calcd for $C_{50}H_{62}{}^{81}Br_4$ 986.1503, found: 986.1509.

4.3. Synthesis of 9,9,9′,9′-tetrakis(3-(1-methylimidazolium-3-yl)hexyl)-2,2′-bifluorene tetrakis(hexafluorophosphate) (**1**)

A mixture of 9,9,9′,9′-tetrakis(3-bromopropyl)-2,2′-bifluorene (693 mg, 0.71 mmol) and 1-methylimidazole (0.24 mL, 3.03 mmol) were dissolved in toluene (3 mL) and refluxed for 16 h. The reaction mixture was concentrated and dissolved in MeOH (3 mL), then poured into $KPF_{6(aq)}$ (30 mL, 0.15 M). The white precipitate was collected by filtration to afford pure **2** (895 mg, 81%) as a white solid. ^1H NMR (DMSO-d_6, 400 MHz) δ8.95 (s, 4H), 7.88 (d, J = 8.0 Hz, 2H), 7.84 (d, J = 8.0 Hz, 2H), 7.83 (s, 2H), 7.74 (d, J = 8.0 Hz, 2H), 7.62 (s, 8H), 7.44 (d, J = 6.4 Hz, 2H), 7.37–7.31 (m, 4H), 4.00 (t, J = 7.2 Hz, 8H), 3.78 (s, 12H), 2.09–2.06 (m, 8H), 1.55 (quin, J = 7.2 Hz, 8H), 1.06–0.96 (m, 16H), 0.57 (m, 8H); ^{13}C NMR (DMSO-d_6, 100 MHz) δ151.4, 150.6, 140.6, 140.4, 139.6, 136.8, 129.3, 128.6, 127.7, 127.4, 126.2, 124.0, 123.3, 122.5, 121.0, 120.7, 120.4, 55.2, 49.1, 36.1, 29.7, 25.8, 24.0; HRMS (m/z, FAB^+) Calcd for $C_{66}H_{86}N_8^{4+}$ 990.6954, found: 990.6976.

4.4. Fabrication and characterization of LEC devices

ITO-coated glass (AimCore Tech.) substrates were cleaned and treated with UV/ozone prior to use. A PEDOT:PSS (H.C. Starck Clevios GmbH) layer was spin-coated

at 4000 rpm for 60 s onto the ITO substrate in air and then the structure was baked at 150 °C for 30 min. For Device **I**, the emissive layer (250 nm) was spin-coated from an acetonitrile solution of **1**. For Device **II**–**IV**, the emissive layers were spin-coated from a mixed acetonitrile solution containing a mass ratio of **1**:PMMA = 0.9:0.1 with concentrations of 150, 200 and 250 mg/mL, respectively. The spin rate and time for spin coating of the emissive layer are 3000 rpm and 60 s, respectively. The PMMA (average *M.W* = 350,000) used in this work was purchased from Alfa Aesar and was used as received. The thicknesses of the emissive layers of Devices **II**–**IV** are 250, 350 and 500 nm, respectively. All solution preparing and spin-coating processes were carried out under ambient conditions. After spin-coating the emissive layer, the samples were baked at 70 °C for 10 h in a nitrogen glove box (oxygen and moisture levels below 1 ppm) and then subjected to thermal evaporation of a 100 nm thick Ag top contact in a vacuum chamber (*ca.* 10^{-6} torr). The electrical and emission characteristics of the LEC devices were measured using a source-measurement unit and a Si photodiode calibrated with a Photo Research PR-650 spectroradiometer. All device measurements were performed under a constant bias voltage in a nitrogen glove box. EL spectra of LEC devices were recorded using a calibrated CCD spectrograph.

Acknowledgements

The authors gratefully acknowledge the financial support from the National Science Council of Taiwan. Experiments and technical assistant of Technology Commons, College of Life Science and Precision Instrumentation Center, NTU with CLSM and TEM analysis.

References

[1] (a) Q. Pei, G. Yu, C. Zhang, Y. Yang, A.J. Heeger, Science 269 (1995) 1086;
(b) Q. Pei, Y. Yang, G. Yu, C. Zhang, A.J. Heeger, J. Am. Chem. Soc. 118 (1996) 3922;
(c) V. Cimrová, W. Schmidt, R. Rulkens, M. Schulze, W. Meyer, D. Neher, Adv. Mater. 8 (1996) 585;
(d) L. Edman, M. Pauchard, B. Liu, G. Bazan, D. Moses, A.J. Heeger, Appl. Phys. Lett. 82 (2003) 3961;
(e) D. Vak, S.-H. Oh, D.-Y. Kim, Appl. Phys. Lett. 94 (2009) 243305.
[2] (a) S. Alem, J. Gao, Org. Electron. 9 (2008) 347;
(b) Y. Hu, J. Gao, J. Am. Chem. Soc. 133 (2011) 2227;
(c) S. van Reenen, P. Matyba, A. Dzwilewski, R.A.J. Janssen, L. Edman, M. Kemerink, J. Am. Chem. Soc. 132 (2010) 13776;
(d) J. Fang, P. Matyba, N.D. Robinson, L. Edman, J. Am. Chem. Soc. 130 (2008) 4562.
[3] (a) C.H. Lyons, E.D. Abbas, J.K. Lee, M.F. Rubner, J. Am. Chem. Soc. 120 (1998) 12100;
(b) F.G. Gao, A.J. Bard, J. Am. Chem. Soc. 122 (2000) 7426;
(c) J.D. Slinker, J. Rivnay, J.S. Moskowitz, J.B. Parker, S. Bernhard, H.D. Abruña, G.G. Malliaras, J. Mater. Chem. 17 (2007) 2976.
[4] (a) A.B. Tamayo, S. Garon, T. Sajoto, P.I. Djurovich, I.M. Tsyba, R. Bau, M.E. Thompson, Inorg. Chem. 44 (2005) 8723;
(b) J.D. Slinker, A.A. Gorodetsky, M.S. Lowry, J. Wang, S. Parker, R. Rohl, S. Bernhard, G.G. Malliaras, J. Am. Chem. Soc. 126 (2004) 2763;
(c) H.-C. Su, H.-F. Chen, Y.-C. Shen, C.-T. Liao, K.-T. Wong, J. Mater. Chem. 21 (2011) 9653;
(d) H.-F. Chen, K.-T. Wong, Y.-H. Liu, Y. Wang, Y.-M. Cheng, M.-W. Chung, P.-T. Chou, H.-C. Su, J. Mater. Chem. 21 (2011) 768;
(e) J.K. Lee, D.S. Yoo, E.S. Handy, M.F. Rubner, Appl. Phys. Lett. 69 (1996) 1686;
(f) D. Tordera, S. Meier, M. Lenes, R.D. Costa, E. Ortí, W. Sarfert, H.J. Bolink, Adv. Mater. 24 (2012) 897;
(g) H.-C. Su, H.-F. Chen, C.-C. Wu, K.-T. Wong, Asian J. Chem. 3 (2008) 1922;
(h) G. Kalyuzhny, M. Buda, J. McNeill, P. Barbara, A.J. Bard, J. Am. Chem. Soc. 125 (2003) 6272;
(i) K.W. Lee, J.D. Slinker, A.A. Gorodetsky, S. Flores-Torres, H.D. Abruña, P.L. Houston, G.G. Malliaras, Phys. Chem. Chem. Phys. 5 (2003) 2706;
(j) T. Hu, L. He, L. Duan, Y. Qiu, J. Mater. Chem. 22 (2012) 4206;
(k) F. Dumur, D. Bertin, D. Gigmes, Int. J. Nanotechnol. 9 (2012) 377.
[5] (a) K.A. King, R.J. Watts, J. Am. Chem. Soc. 109 (1987) 1589;
(b) S. Lamansky, P. Djurovich, D. Murphy, F.A. Razzaq, R. Kwong, I. Tsyba, M. Bortz, B. Mui, R. Bau, M.E. Thompson, Inorg. Chem. 40 (2001) 1704;
(c) T. Sajoto, P.I. Djurovich, A. Tamayo, M. Yousufuddin, R. Bau, M.E. Thompson, Inorg. Chem. 44 (2005) 7992.
[6] H.-F. Chen, C.-T. Liao, T.-C. Chen, H.-C. Su, K.-T. Wong, T.-F. Guo, J. Mater. Chem. 21 (2011) 4175.
[7] (a) M.A. Baldo, S. Lamansky, P.E. Burrows, M.E. Thompson, S.R. Forrest, Appl. Phys. Lett. 75 (1999) 4;
(b) R.J. Holmes, S.R. Forrest, Y.-J. Tung, R.C. Kwong, J.J. Brown, S. Garon, M.E. Thompson, Appl. Phys. Lett. 82 (2003) 2422;
(c) S. Tokito, T. Iijima, T. Tsuzuki, F. Sato, Appl. Phys. Lett. 83 (2003) 2459;
(d) S.-J. Yeh, M.-F. Wu, C.-T. Chen, Y.-H. Song, Y. Chi, M.-H. Ho, S.-F. Hsu, C.H. Chen, Adv. Mater. 17 (2005) 285.
[8] (a) R.J. Holmes, B.W. D'Andrade, S.R. Forrest, X. Ren, J. Li, M.E. Thompson, Appl. Phys. Lett. 83 (2003) 3818;
(b) X. Ren, J. Li, R.J. Holmes, P.I. Djurovich, S.R. Forrest, M.E. Thompson, Chem. Mater. 16 (2004) 4734.
[9] (a) T.-C. Chao, Y.-T. Lin, C.-Y. Yang, T.-S. Hung, H.-C. Chou, C.-C. Wu, K.-T. Wong, Adv. Mater. 17 (2005) 992;
(b) K.-T. Wong, Y.-L. Liao, Y.-T. Lin, H.-C. Su, C.-C. Wu, Org. Lett. 7 (2005) 5131.
[10] K.L. Billingsley, T.E. Barder, S.L. Buchwald, Angew. Chem. Int. Ed. 46 (2007) 5359.
[11] B. Liu, B.S. Gaylord, S. Wang, G.C. Bazan, J. Am. Chem. Soc. 125 (2003) 6705.
[12] H. Rudmann, S. Shimada, M.F. Rubner, J. Am. Chem. Soc. 124 (2002) 4918.
[13] V. Bulovic, A. Shoustikov, M.A. Baldo, E. Bose, V.G. Kozlov, M.E. Thompson, S.R. Forrest, Chem. Phys. Lett. 287 (1998) 455.
[14] (a) L. Wang, H. Liu, J. Hao, Chem. Commun. (2009) 1353;
(b) C.J. Medforth, Z. Wang, K.E. Martin, Y. Song, J.L. Jacobsenc, J.A. Shelnutt, Chem. Commun. (2009) 7261.
[15] H. Rudmann, M.F. Rubner, J. Appl. Phys. 90 (2001) 4338.
[16] K. Kalyanasundaram, J.K. Thomas, J. Am. Chem. Soc. 99 (1977) 2039.
[17] J.-P. Choi, K.-T. Wong, Y.-M. Chen, J.-K. Yu, P.-T. Chou, A.J. Bard, J. Phys. Chem. B 107 (2003) 14407.
[18] (a) S.T. Parker, J.D. Slinker, M.S. Lowry, M.P. Cox, S. Bernhard, G.G. Malliaras, Chem. Mater. 17 (2005) 3187;
(b) Y. Ohsawa, S. Sprouse, K.A. King, M.K. DeArmond, K.W. Hanck, R.J. Watts, J. Phys. Chem. 91 (1987) 1047;
(c) J.-H. Shin, S. Xiao, L. Edman, Adv. Funct. Mater. 16 (2006) 949;
(d) Y. Shao, X. Gong, A.J. Heeger, M. Liu, A.K.-Y. Jen, Adv. Mater. 21 (2009) 1972;
(e) U. Scherf, E.J.W. List, Adv. Mater. 14 (2002) 477.
[19] M. Hernández-Guerrero, M.H. Stenzel, Polym. Chem. 3 (2012) 563.
[20] P.B. Shea, C. Chen, J. Kanicki, L.R. Pattison, P. Petroff, H. Yamada, N. Ono, Appl. Phys. Lett. 90 (2007) 233107.